AMERICAN SOCIETY FOR MICROBIOLOGY | Journal of Virology®

PATHOGENESIS AND IMMUNITY

Zika Virus Mucosal Infection Provides Protective Immunity

Laura E. Martínez,[a] Gustavo Garcia, Jr.,[a] Deisy Contreras,[b] Danyang Gong,[a] Ren Sun,[a,c] Vaithilingaraja Arumugaswami[a,b,d]

[a]Department of Molecular and Medical Pharmacology, University of California, Los Angeles, California, USA
[b]Department of Surgery, Cedars-Sinai Medical Center, Los Angeles, California, USA
[c]Molecular Biology Institute, University of California, Los Angeles, California, USA
[d]Eli and Edythe Broad Center of Regenerative Medicine and Stem Cell Research, University of California, Los Angeles, California, USA

ABSTRACT Zika virus (ZIKV) is a major human pathogen. ZIKV can replicate in female and male reproductive organs, thus facilitating the human-human transmission cycle. Viral shedding in the semen can increase the risk of ZIKV transmission through sexual mode. Therefore, the vaginal and anorectal mucosa are relevant sites for ZIKV infection. However, the pathobiology of ZIKV transmission through the rectal route is not well understood. Here, we utilize a mouse model system to investigate the immunopathological consequences following ZIKV infection of the rectal mucosa compared to a subcutaneous route of infection. We show that ZIKV-rectal inoculation results in viremia with subclinical infection. ZIKV infects the mucosal epithelium and submucosal dendritic cells, inducing immune and inflammatory cell infiltration. Rectal transmission of ZIKV resulted in the generation of serum-neutralizing antibody responses. Mass cytometry analyses of splenocytes showed a significantly reduced level of inflammatory monocyte and neutrophil cellular responses in the rectal route group. Furthermore, immunological priming through the rectal mucosa with an attenuated ZIKV strain resulted in significant protection from lethal subcutaneous ZIKV challenge, further eliciting robust memory CD4-positive ($CD4^+$) and $CD8^+$ T-cell and ZIKV-specific serum-neutralizing antibody responses. Thus, our study provides deeper immunopathobiological insights on rectal transmission and highlights a rational strategy for mucosal immunization. This model system recapitulates clinical aspects of human ZIKV disease outcome, where most infections are well controlled and result in subclinical and asymptomatic outcomes.

IMPORTANCE Zika virus is a clinically significant human pathogen that is primarily transmitted and spread by *Aedes* species mosquitoes but is also sexually transmissible. The recent pandemic in the Americas led to an unprecedented increase of newborn babies with developmental brain and eye abnormalities. To date, there is no licensed vaccine or therapeutic intervention available for the fight against ZIKV. Understanding the sexual transmission of ZIKV through vaginal and rectal routes is necessary to restrict virus transmission and spread. This study examines the early immunological and pathological consequences of rectal and subcutaneous routes of ZIKV infection using a mouse model. We characterized the primary target cells of ZIKV infection and the subsequent mucosal immune responses to infection, and we demonstrate the protective effect of mucosal rectal immunization using an attenuated ZIKV strain. This mucosal vaccination approach can be further developed to prevent future ZIKV outbreaks.

KEYWORDS Zika virus, immunization, rectal infection

Zika virus (ZIKV) is a major human pathogen which belongs to the family of *Flaviviridae*. Vertical transmission of ZIKV in infected mothers causes microcephaly and congenital eye disease (1–4). Sexual transmission of ZIKV has been reported

Citation Martínez LE, Garcia G, Jr, Contreras D, Gong D, Sun R, Arumugaswami V. 2020. Zika virus mucosal infection provides protective immunity. J Virol 94:e00067-20. https://doi.org/10.1128/JVI.00067-20.

Editor Jae U. Jung, University of Southern California

Address correspondence to Vaithilingaraja Arumugaswami, VArumugaswami@mednet.ucla.edu.

Received 13 January 2020
Accepted 4 February 2020
Accepted manuscript posted online 12 February 2020
Published 16 April 2020

between males to females (5–7) and males to males, (8) and there was a suspected case of female-to-male transmission (9). Several studies have reported infectious ZIKV in semen (10–14) months after symptom onset (15–18). The presence of ZIKV in semen and bodily fluids can enhance the risk of sexual transmission. ZIKV infection of the rectal mucosa and the mechanisms governing its immunopathogenesis are poorly understood.

Mouse models of Zika virus pathogenesis have shown that mice deficient in type I interferon (IFN) receptor (*Ifnar1*$^{-/-}$ or A129) signaling pathway develop neurological disease in adults and congenital infection in pregnant females (19–22). Adult immunocompetent (wild-type) mice are resistant to ZIKV infection due to a robust innate immune response that limits infection and spread. Thus, the *Ifnar1*$^{-/-}$ mouse model has become a widely used *in vivo* model system to investigate the pathogenesis of ZIKV-mediated disease. Subcutaneous or intravaginal ZIKV infection of *Ifnar1*$^{-/-}$ female mice causes the activation of systemic and localized immune responses and the establishment of congenital and neurological diseases (21, 23, 24). Vaginal exposure of ZIKV during the first trimester of pregnancy in wild-type mice leads to brain infection, fetal growth restriction, and, in some cases, loss of pregnancy (24). In *Ifnar1*$^{-/-}$ male mice, ZIKV robustly infects the brain, spinal cord, and testes (20). Others have shown that ZIKV causes injury in the testes and epididymis, further reducing the levels of testosterone and oligospermia (25). ZIKV can also cause testicular atrophy following 21 days of subcutaneous infection (26), which may lead to infertility (27). Moreover, ZIKV-infected epididymal epithelial cells are the predominant source of infectious cell-free virus shed in the seminal fluid of the murine male reproductive tract (28). ZIKV is also capable of infecting and efficiently replicating in human Sertoli cells (29, 30). ZIKV-infected patients have elevated levels of chemokines, including monocyte chemoattractant protein 1 (MCP-1 or CCL2) and CXCL10 (31, 32).

Intraperitoneally infected AG129 (interferon-α/β and -γ receptor knockout) male mice exhibited persistent testicular infection for more than a month, and the semen contained infectious ZIKV at 1 to 3 weeks postinoculation (33). In addition, ZIKV infection was documented in 50% of female mice mated to infected nonvasectomized male mice (33). These mouse models of ZIKV infection suggest that males carry infectious virus longer than females. Others have shown that the innate immune cell responders to acute infection of pigtail macaques are dendritic cells, monocytes, and neutrophils following subcutaneous ZIKV infection (34). These cell responders are significantly higher in male macaques and correlate with increased viral persistence in peripheral lymph nodes and mucosal tissues, such as the colon and rectum.

ZIKV has been detected in rectal swab samples (35) and in a stool sample from an acutely infected patient (36). *In vivo*, intrarectal inoculation with ZIKV in rhesus and cynomolgus macaques leads to detectable viremic levels 21 days postinoculation and with seroconversion (37). The duration of infectious virus in the blood after a few weeks suggests that infection in humans could generate viremia sufficient to infect others through this route. Moreover, Li et al. showed that intra-anal inoculation with ZIKV leads to robust infection of *Ifnar*$^{-/-}$ and immunocompetent mice, eliciting innate and humoral immune responses (36). In addition, rectal inoculation of ZIKV in pregnant mice results in transplacental infection and delayed fetal development.

Although systemic viral replication kinetics in various tissues following rectal ZIKV inoculation have been reported, the *in vivo* primary cell types supporting ZIKV infection and/or replication at the rectal mucosa and associated early mucosal immune and inflammatory events, as well as systemic-splenic immune responses, remain largely unknown. Moreover, it is critical to understand the mucosal immune responses elicited against ZIKV, which can provide systemic immune protection. This knowledge can lead to developing effective and preventive immunization strategies against ZIKV.

RESULTS

The rectal route of ZIKV inoculation establishes systemic infection and disseminates to reproductive organs. In this study, we examined the early events following

rectal and subcutaneous ZIKV inoculations. We used 4- to 6-week-old mice to determine the pathogenesis of the contemporary Zika virus strain PRVABC59 (isolated in Puerto Rico in 2015) following rectal inoculation and followed disease progression for 21 days postinoculation (dpi). We utilized the *Ifnar1*$^{-/-}$ mouse model system, as it supports ZIKV replication, tissue damage, and an adverse neurological disease phenotype that can be used to compare sexual (rectal) and mosquito (subcutaneous) modes of transmission and their resulting systemic and mucosal response to infection. Because the virus inoculation site and dose may affect the outcome of ZIKV transmission and pathogenesis, we inoculated mice via rectal and subcutaneous routes using the same viral dose (1×10^6 PFU/mouse). Weight loss and neurological signs were monitored at various times during the course of infection. Rectal inoculation of ZIKV did not cause mortality in *Ifnar1*$^{-/-}$ mice (Fig. 1A). Two of five infected mice showed lethargy and transient sickness, with reduced body weight (~12 to 14%) at 10 dpi (Fig. 1B). Mice steadily recovered body weight by 14 dpi. Rectally infected mice did not show signs of enteric disease such as diarrhea or soiled hindquarters. In addition, mice had high viremic levels at 3 and 7 dpi and detectable viremia at 21 dpi (Fig. 1C).

Subcutaneous ZIKV inoculation led to robust systemic viral spread as measured by significantly higher viremia (10^4 mean genome copies) (Fig. 1D). Consistent with previous reports using *Ifnar1*$^{-/-}$ mice (38), mice infected by the subcutaneous route demonstrated significant weight loss and exhibited malaise, incoordination, and neurological signs of posterior hind-leg paralysis (2 of 6 infected mice) requiring euthanasia. Rectally infected mice displayed delayed kinetics of infection, where viremic levels did not increase until 3 dpi (10^5 mean genome copies) but were sustained at 7 dpi compared to the subcutaneous infected group (Fig. 1D). To compare ZIKV tissue tropism and virus dissemination after rectal and subcutaneous inoculations, we measured ZIKV genome copies in the rectum and various tissues, such as the skin, testes, seminal vesicles, brain, and lymph nodes at 1, 3, and 7 dpi by reverse transcriptase quantitative PCR (RT-qPCR). Similar viral loads were observed in the rectum between the two groups (Fig. 1E). Subcutaneously infected mice showed significantly higher viral loads in skin tissue near the inoculation site at 1 dpi (Fig. 1F). Distinct infection kinetics were observed in the testes and seminal vesicles following rectal inoculation (Fig. 1G and H). The rectal group had reduced viral loads in the brain compared to the subcutaneous group at 3 and 7 dpi (Fig. 1I). Despite detectable infection of the brain at 7 dpi, mice did not exhibit neurological signs of disease (weakness of limbs, hind-limb paralysis [paraplegia or hemiplegia], and seizures) following rectal ZIKV inoculation. These results suggest that in our experimental system, ZIKV causes a fundamentally distinct disease outcome in rectally infected mice with a reduced neuroinvasive phenotype. Furthermore, we found that ZIKV disseminates to lymph nodes, including inguinal (Fig. 1J) and mesenteric lymph nodes and the thymus (data not shown). Viral loads in the rectum, testes, and brain persisted for at least 21 days following rectal inoculation (Fig. 1K).

Female mice infected by the rectal route did not show differences from male mice in ZIKV dissemination to local and distant tissue sites. Thus, comparable viral loads were observed in the rectum, brain, spleen, and inguinal and mesenteric lymph nodes at 7 dpi (Fig. 1L). In addition, ZIKV disseminated to the uterus (Fig. 1L), implicating the uterus as a replicative site for ZIKV following rectal transmission, which can increase the risk for *in utero* infection during pregnancy. Overall, our data show that ZIKV disseminates to various tissue sites following rectal inoculation, including the skin, lymph nodes, spleen, and uterus. Similar to Li et al., we found that ZIKV persistently infects the rectum and testes (36).

ZIKV infects the mucosal epithelium and residential dendritic cells. We evaluated the early events of ZIKV infection and performed immunohistochemistry on serial rectal tissue sections (7 to 10 μm thick) using an antibody against the epithelial cell adhesion molecule EpCAM and a rabbit polyclonal antibody recognizing the flavivirus envelope (Env) of ZIKV. We found that ZIKV infects rectal epithelial cells within the

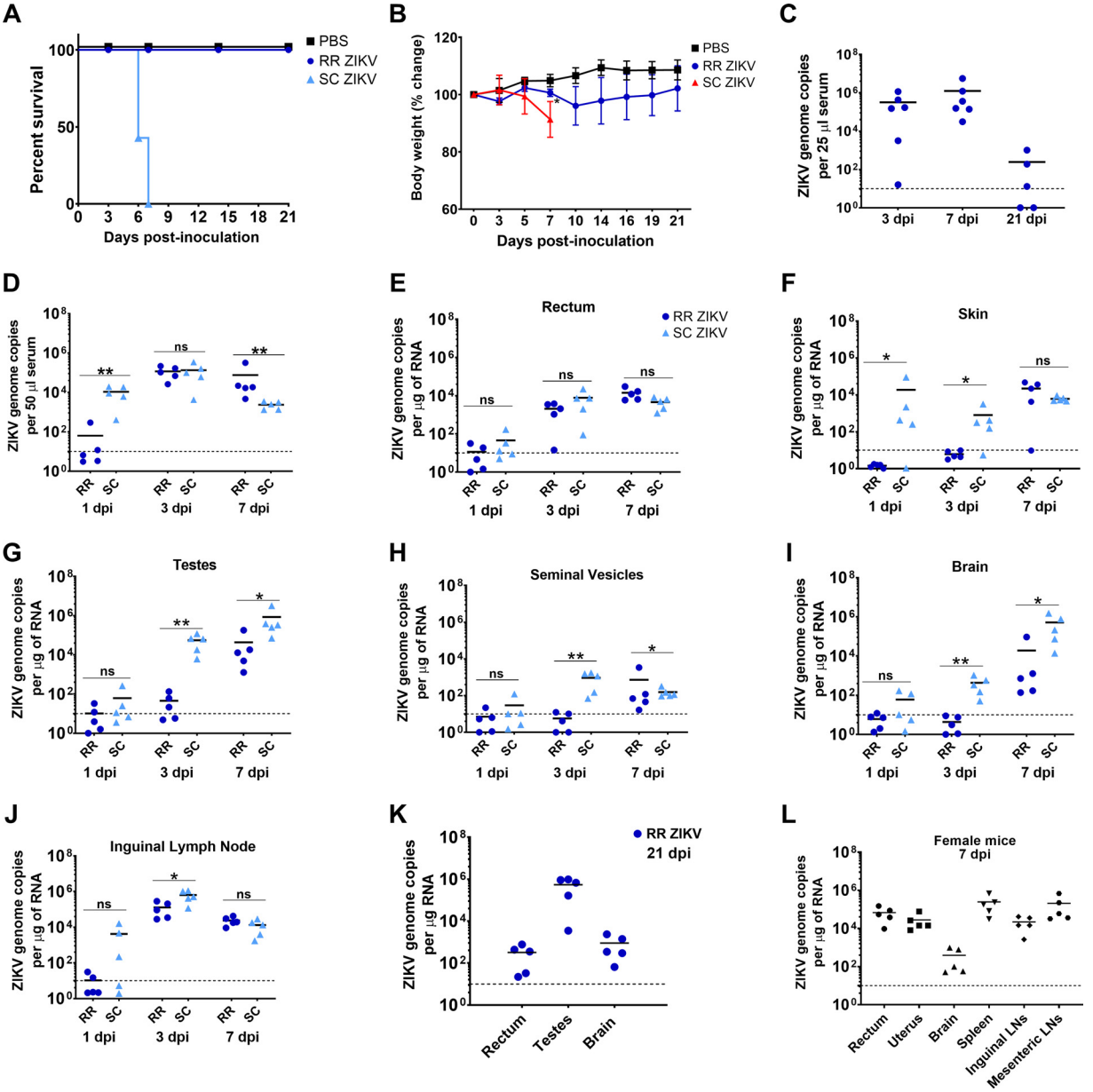

FIG 1 Rectal inoculation of ZIKV in *Ifnar1*$^{-/-}$ mice results in a nonlethal, self-limiting, and differential disseminating infection relative to subcutaneous ZIKV infection. (A) Kaplan-Meier survival plot showing the percent survival of *Ifnar1*$^{-/-}$ male mice postrectal inoculation with PBS ($n = 5$) or ZIKV ($n = 6$) (RR ZIKV) and postsubcutaneous ZIKV inoculation (SC ZIKV) ($n = 6$). (B) Percent body weight change of mice postrectal inoculation. Error bars represent the standard deviation (SD). (C) Viremia of infected mice via the rectal route (RR ZIKV) at days 3, 7, and 21 postinoculation (dpi). Each symbol represents one mouse, with means represented by black lines. Broken lines represent the limit of detection at 10 genome copies per microgram of RNA. (D) Viremia of mice infected through rectal (RR) or subcutaneous routes (SC) at days 1, 3, and 7 postinoculation (dpi). ZIKV genome copies detected in rectum (E), skin (F), testes (G), seminal vesicles (H), brain (I), and inguinal lymph node (J) tissues by RT-qPCR following 1, 3, and 7 days postrectal or subcutaneous inoculations with ZIKV. Each symbol corresponds to data for an individual mouse ($n = 5$ mice per group). Results are representative of one of four independent experiments. Two-tailed, unpaired, nonparametric Mann-Whitney tests were conducted (*, $P < 0.05$; **, $P < 0.001$; ns, no significance). (K) ZIKV genome copies in rectum, testes, and brain at 21 dpi. (L) Viral loads in rectum, uterus, brain, spleen, and inguinal and mesenteric lymph node tissues of *Ifnar1*$^{-/-}$ female mice at day 7 postrectal ZIKV inoculation.

lamina propria and submucosa layers (Fig. 2A and B). Figure 2B shows specific infection of nonepithelial cells surrounding glands within the lamina propria, which we hypothesized were residential and/or infiltrating immune cells to the site after a day of infection. Similar patterns were observed in infected tissue from the subcutaneous group (Fig. 2C). Rectal epithelial cell infection was also verified by coimmunostaining of ZIKV and CDX2, which is expressed in the nuclei of intestinal epithelial cells (data not shown).

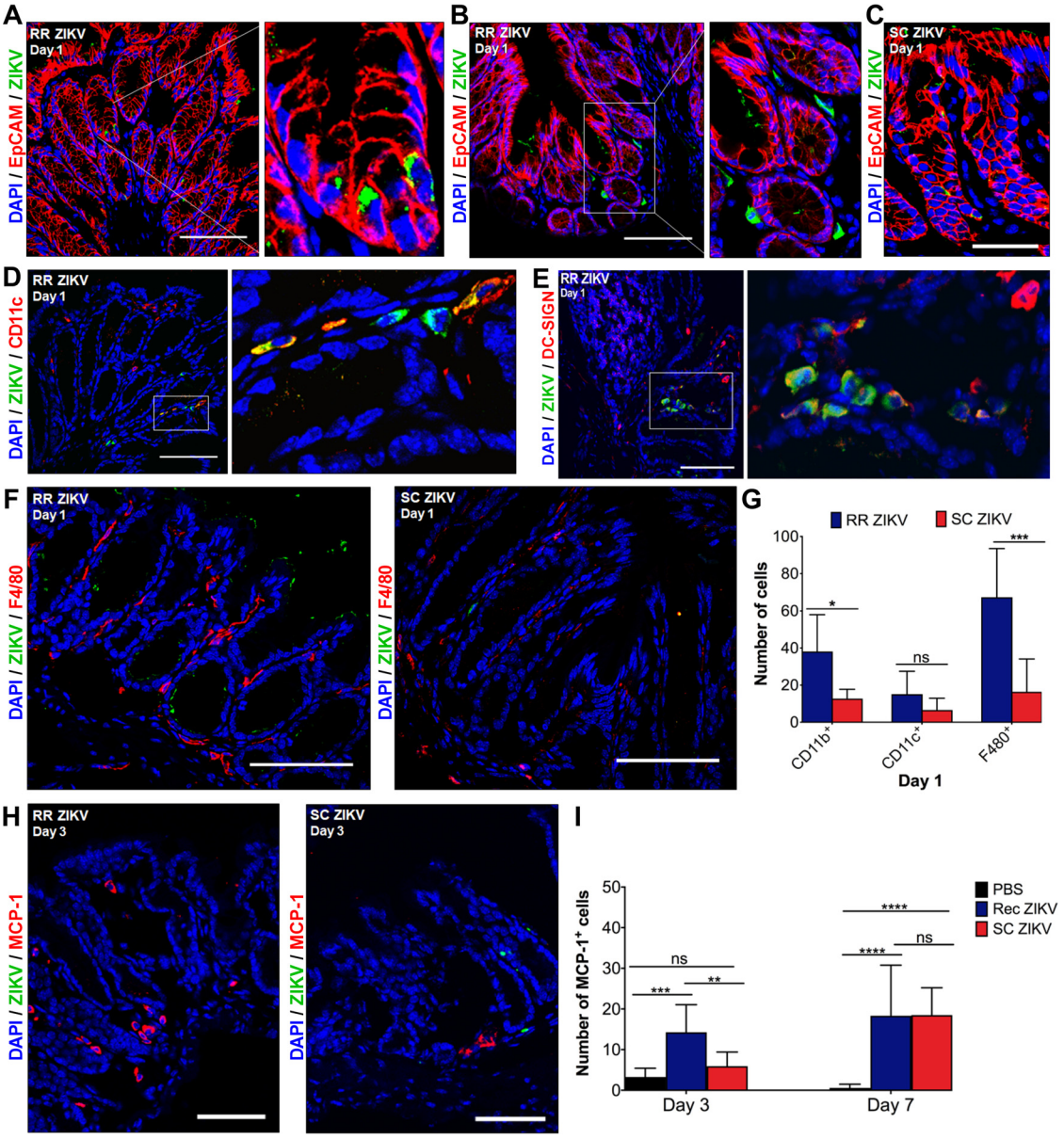

FIG 2 ZIKV infects columnar epithelial cells and dendritic cells in the rectal mucosa 1 day postrectal inoculation. (A, B) Representative immunofluorescence images of rectal tissue from mice infected via the rectal route (RR) at 1 day postinoculation (dpi). Rectal tissue sections were immunostained for EpCAM (red) and ZIKV (green), and nuclei were stained with DAPI (blue). Inset in A shows a magnified view of infected epithelial cells comprising intestinal glands. Inset in B shows a magnified view of infected nonepithelial cells within the lamina propria. (C) Representative image of rectal tissue infected via the subcutaneous route (SC ZIKV) at 1 dpi. (D, E) Representative immunofluorescence images of rectal tissue for RR ZIKV at 1 dpi. Tissue was immunostained for ZIKV (green) and with anti-CD11c (red) or anti-DC-SIGN (red) at 1 dpi. Inset panels show ZIKV-infected CD11c$^+$ or DC-SIGN$^+$ dendritic cells (yellow) within the lamina propria. (F) Images of infected rectal tissue sections for RR and SC ZIKV at 1 dpi. Shown are ZIKV-infected cells (green) and F4/80$^+$ macrophages (red). (G) Quantification of CD11b$^+$, CD11c$^+$, and F4/80$^+$ cells in the rectal mucosa at 1 dpi. (H) MCP-1$^+$ cells in rectal tissue from RR and SC ZIKV at 3 dpi. All images for A to F and H are representative of five different animals per group and were collected at $\times$40 magnification; scale bar, 50 μm. (I) Quantification of MCP-1$^+$ cells for RR and SC ZIKV at 3 and 7 dpi. Multiple-comparison two-way analysis of variance (ANOVA) and Tukey tests were conducted (*, $P < 0.05$; **, $P < 0.001$; ***, $P < 0.0001$; ****, $P < 0.00001$; ns, no significance).

We then immunostained for multiple immune cell subsets using anti-CD11b for monocytes, anti-CD11c or anti-DC-SIGN (dendritic cell-specific intercellular adhesion molecule-3-grabbing nonintegrin) for dendritic cells, anti-F4/80 for macrophages, and anti-CD4 for CD4-positive (CD4$^+$) T cells. We did not observe any specific staining with an IgG isotype control monoclonal antibody utilizing the same secondary antibody used for detection of ZIKV antigen in uninfected (phosphate-buffered saline [PBS]) and

infected tissue sections (data not shown). In addition, no infection was observed in rectal tissue examined for the PBS control group. Uninfected rectal tissue sections revealed immunostaining for residential dendritic cells, monocytes, and macrophages at 1 dpi. We found that ZIKV specifically infects dendritic cells at 1 dpi (Fig. 2D and E).

The rectal route of ZIKV infection leads to enhanced mucosal immune responses. We further characterized the immune cells responding to infection of the rectal mucosa by quantifying the number of monocytes ($CD11b^+$), dendritic cells ($CD11c^+$), macrophages ($F4/80^+$), $CD45^+$ leukocytes, and $CD4^+$ T cells. Serial rectal tissue sections from uninfected and infected tissue samples were used. We observed an increased number of $F4/80^+$ macrophages within the lamina propria of the rectal mucosa of rectally inoculated mice at 1 dpi (Fig. 2F). Further quantification of immune cells within rectal tissue sections revealed increased numbers of $CD11b^+$ monocytes and $F4/80^+$ macrophages in the rectal mucosa of rectally infected mice as early as a day of infection (Fig. 2G). Moreover, rectal ZIKV infection results in an increased monocyte chemoattractant protein-1 (MCP-1) response in the rectal mucosa at 3 dpi relative to the subcutaneous group (Fig. 2H and I). No significant differences in the numbers of monocytes, dendritic cells, and macrophages were observed between the infected groups at 3 dpi (data not shown). However, subcutaneous ZIKV infection resulted in a significant increase in $CD11c^+$ and $CD45^+$ cells in the rectal mucosa at 7 dpi (Fig. 3A and B). Significant numbers of $CD4^+$ T cells were observed for the rectal group at 7 dpi (Fig. 3A). It is possible that besides $CD11c^+$ and $F4/80^+$ cells, other immune subsets (e.g., B cells, NK cells) may be affected as well. We then proceeded to measure the expression of key inflammatory response genes (*IL-6* and *OAS-1*) early after infection of the rectal mucosa at days 1, 3, and 7, including the anti-inflammatory interleukin 10 (*IL-10*). No significant differences in the induction of *IL-6*, *OAS-1*, and *IL-10* were observed in the rectum of the two infected mice groups at 1 dpi (data not shown).

Collectively, these results suggest that there are increased immune responses in the rectal mucosa early after infection. Overall, intestinal epithelial cells and dendritic cells support ZIKV infection in the rectal mucosa following rectal and subcutaneous routes of infection. The early recruitment and secretion of MCP-1^+ cells can mediate the recruitment of additional immune cell infiltrates to the site of infection.

The brain is differentially affected in rectal versus subcutaneous modes of ZIKV transmission. We then explored the differential brain pathogenesis induced by rectal and subcutaneous routes of ZIKV infection. We detected fewer infected cells in the brains of the rectal route (RR) ZIKV group with no remarkable histopathological alterations (Fig. 4A, bottom). Diffuse and focal areas of ZIKV infection in the brain parenchyma were observed in the subcutaneous group (Fig. 4A). In addition, reduced levels of apoptotic brain cells were observed in the RR ZIKV group as determined by reduced cleaved caspase-3 activity through immunofluorescence assay (Fig. 4B). We then examined the mice brains at an earlier time point of infection. ZIKV reached the blood-brain barrier and infected brain microvascular endothelial cells and astrocytes at 1 dpi, as assessed by immunostaining of CD31 and glial fibrillary acidic protein (GFAP), respectively (Fig. 4C). We also found that MCP-1 was expressed in cells early after infection at 1 dpi and during late-onset acute infection at 7 dpi (Fig. 4D and E). In addition, $GFAP^+$ astrocytes were a main source of cytokine-induced MCP-1 in the brain (Fig. 4E).

We then observed that ZIKV elicited comparable *IL-6*, *IL-10*, and *MCP-1* responses in the brains of RR and subcutaneous (SC) ZIKV mice at 1 and 3 dpi (Fig. 4F). A significantly higher *OAS-1* response was observed at 3 dpi for the SC ZIKV group. Furthermore, subcutaneous infection resulted in significantly higher *IL-10* and *MCP-1* responses in mice by 7 dpi, which correlate with higher inflammatory cell infiltrates and apoptotic patterns observed at this time point.

Systemic immunophenotyping reveals higher $CD4^+$ and $CD8^+$ T-cell responses early on following the rectal route of ZIKV infection. Our results indicate that rectal ZIKV inoculation leads to subclinical infection with a reduced neuroinvasive phenotype compared to a subcutaneous route of infection. It is possible that differential immune

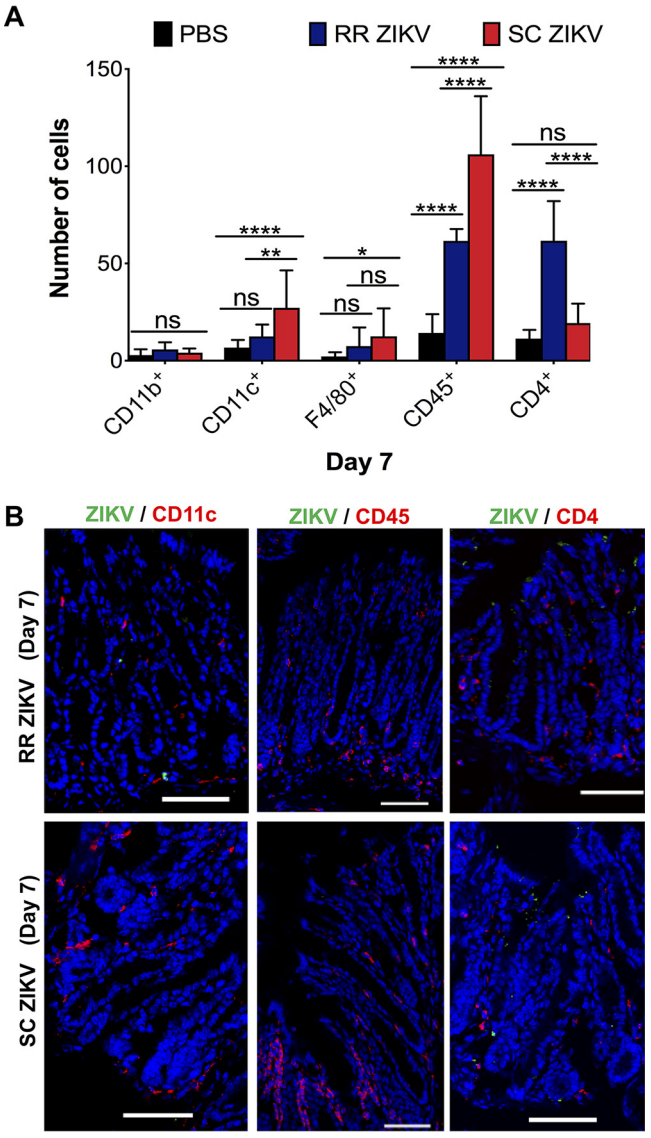

FIG 3 Rectal route of ZIKV infection results in increased $CD4^+$ T-cell responses in the rectal mucosa. (A) Quantification of $CD11b^+$ monocytes, $CD11c^+$ dendritic cells, $F4/80^+$ macrophages, $CD45^+$ leukocytes, and $CD4^+$ T cells in the rectal mucosa of uninfected (PBS) and RR and SC ZIKV-infected groups at 7 dpi. (B) Infected rectal tissue sections immunostained for ZIKV and anti-CD11c, ZIKV and anti-CD45, or ZIKV and anti-CD4 for RR and SC ZIKV groups at 7 dpi. For A, multiple-comparison two-way ANOVA and Tukey tests were conducted (*, $P < 0.05$; **, $P < 0.001$; ***, $P < 0.0001$; ****, $P < 0.00001$; ns, no significance). Data are representative of one of four independent experiments.

responses can contribute to the clinical outcomes following different routes of transmission. Subsequently, we probed the immune response to ZIKV infection in the spleens of mice, a site important for local and systemic regulation of immunity and filtering blood-borne pathogens. Significantly greater viral loads were observed in the SC ZIKV group at 3 dpi but not at 7 dpi (Fig. 5A). However, significantly higher spleen weights were observed for the RR ZIKV group at 7 dpi, which resulted in splenomegaly (Fig. 5B and C). We performed mass cytometry for high-dimensional profiling of different leukocytes (neutrophils, macrophages, dendritic cells, T cells, and B cells) in response to rectal and subcutaneous routes of infection. Cells were stained with epitope-specific antibodies (CD3, CD11b, CD11c, CD45, CD8a, CD4, CD45R, Ly-6C, Ly-6G, CD80, and CD19) conjugated to transition element isotopes as summarized in Table 1. Comprehensive analyses of various immune cell populations were summarized by multidimensional t-distributed stochastic neighbor embedding (t-SNE) plots, which

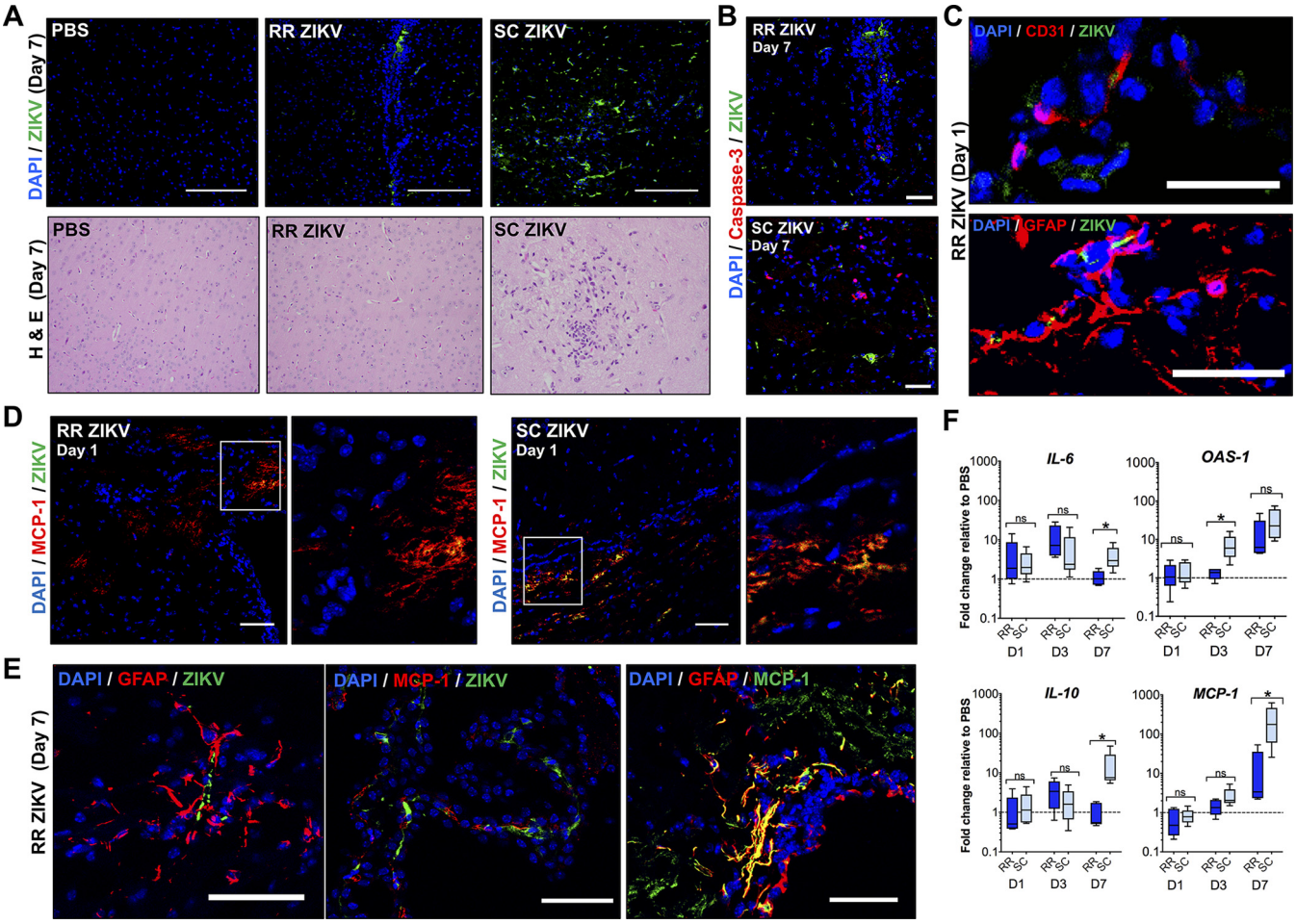

FIG 4 Rectal ZIKV inoculation leads to reduced pathology and inflammation in the brain. (A, Top) Immunofluorescence images of uninfected (PBS) and infected brain tissue sections at 7 dpi (RR versus SC routes). Tissues were immunostained with anti-flavivirus antibody (green), and nuclei were stained with DAPI (blue). (A, Bottom) H&E images of brain tissue sections at 7 dpi (×10 objective). (B) Immunofluorescence images showing ZIKV infection (green) and cleaved caspase-3 immunostaining (red) of infected brain sections at 7 dpi. Images were collected at ×40 magnification; scale bar, 50 μm. (C) Images of ZIKV-infected CD31$^+$ endothelial cells (top) and infected GFAP$^+$ astrocytes (bottom) for RR ZIKV brain sections at 1 dpi. Images were collected at ×20 magnification; scale bar, 20 μm. (D) Immunofluorescence images showing ZIKV infection (green) and MCP-1$^+$ cells (red) in RR or SC ZIKV-infected brains at 1 dpi. Images were collected at ×20 magnification; scale bar, 50 μm. (E) ZIKV-infected GFAP$^+$ astrocytes (left), infected MCP-1$^+$ cells (middle), and colocalization of MCP-1$^+$ with GFAP$^+$ cells (right) at 7 dpi. Images were collected at ×20 magnification; scale bar, 50 μm. (F) Fold change of *IL-6*, *OAS-1*, *IL-10*, and *MCP-1* in the brain relative to the PBS control group at days 1, 3, and 7. Two-tailed unpaired, nonparametric Mann-Whitney tests were conducted (*, $P < 0.05$; **, $P < 0.001$; ns, no significance). Data are representative of one of two independent experiments.

show global dynamic changes during mucosal and systemic routes of inoculation at days 3 and 7 (Fig. 5D). Gating and cell identification strategies recommended for mass cytometry were implemented. Leukocytes were differentiated by the expression of CD45, and different immune cell types were subgated from CD45$^+$ cells, based on the expression of specific immune cell markers.

We found a significantly higher inflammatory response in the subcutaneous ZIKV group at 3 dpi, where higher percentages of neutrophils, monocytes, and dendritic cells were observed than those of rectal ZIKV group (Fig. 5E). The SC ZIKV-infected group showed significantly lower CD4$^+$ and CD8$^+$ T-cell responses at 3 dpi but stronger T-cell responses at 7 dpi (Fig. 5E). Moreover, we found that mucosal infection elicited ZIKV-specific neutralizing serum antibody responses at 20 dpi (Fig. 5F), which could limit virus replication and spread and reduce tissue pathology.

Rectal ZIKV mucosal priming results in developing protective immunity. In order to study the protective nature of mucosal-induced immune responses, we immunized mice by rectal inoculation for 21 days and then challenged mice with ZIKV via subcutaneous route. We used a wild-type ZIKV PRVABC59 strain and a previously

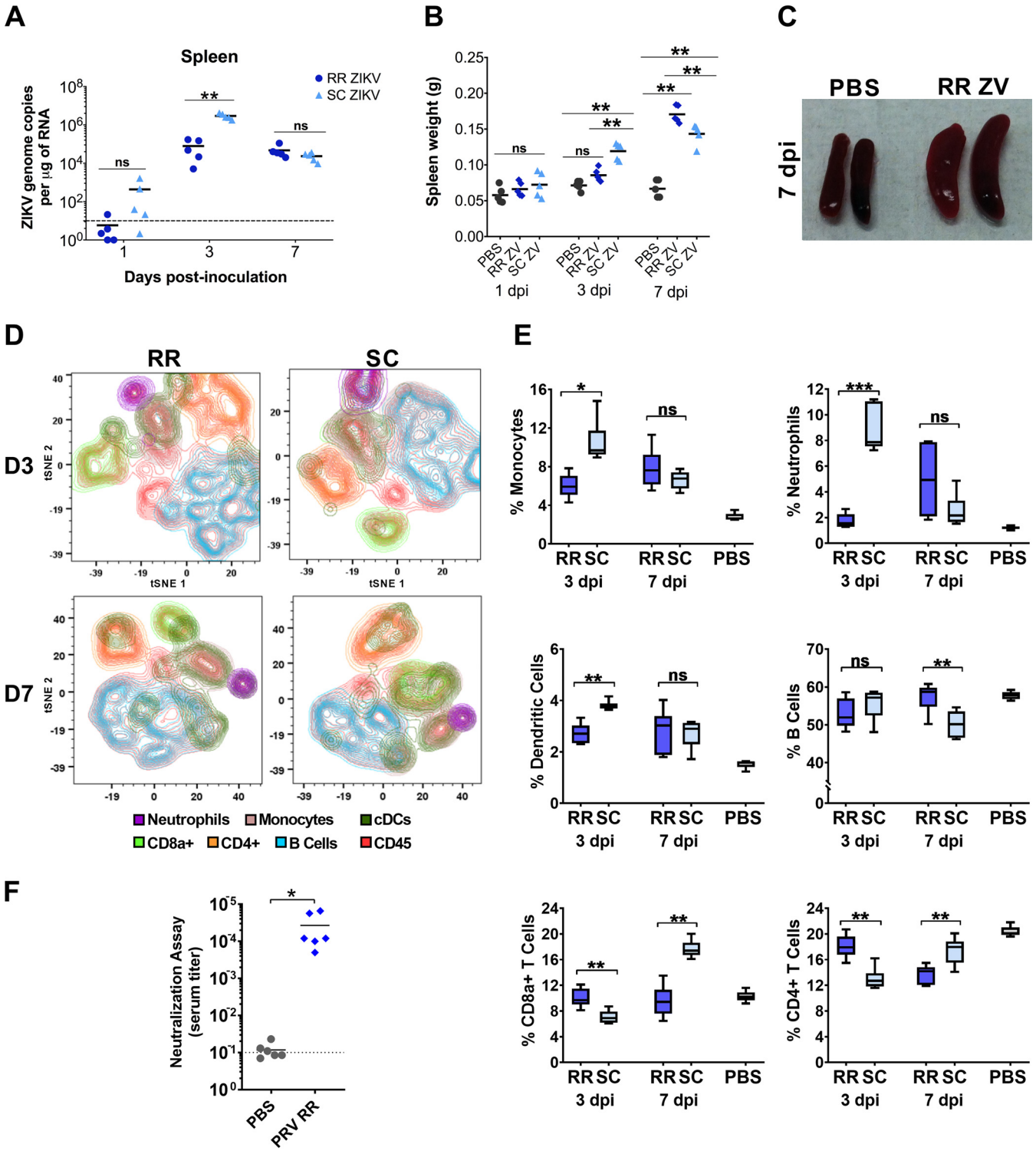

FIG 5 Systemic cellular and humoral immune responses following rectal and subcutaneous routes of ZIKV infection. (A) ZIKV genome copies in the spleen, and (B) spleen weights determined at days 1, 3, and 7 postrectal (RR ZIKV) or subcutaneous ZIKV (SC ZIKV) inoculations. For A and B, two-tailed unpaired, nonparametric Mann-Whitney tests were conducted (*, $P < 0.05$; **, $P < 0.001$; ns, no significance). (C) Gross images of uninfected (PBS) and infected (RR ZIKV) spleens at 7 dpi. (D) Spleen cells were stained with metal-conjugated antibodies and metal intercalators (rhodium and iridium) (as provided in Table 1) and analyzed by mass cytometry. t-SNE plots showing spatially distinct immune cell populations in the spleens of mice following rectal (RR) or subcutaneous (SC) ZIKV inoculations at days 3 (D3) and 7 (D7). (E) The percentage of monocytes ($CD45^+$ $CD11b^+$), neutrophils ($CD45^+$ $Ly6G^+$ $CD11b^+$), dendritic cells ($CD45^+$ CD317 negative [$CD317^-$] $CD11c^+$), B cells ($CD45^+$ $CD3^-$ $CD19^+$), and $CD8^+$ and $CD4^+$ T cells ($CD45^+$ $CD3^+$) following RR and SC ZIKV inoculations at 3 and 7 dpi. As a reference, splenic cell populations quantified for PBS control mice (day 7 following PBS inoculation via rectal and subcutaneous routes) were included. (F) Prechallenge serum neutralization titer of control mice (PBS) and ZIKV (PRVABC59)-infected mice via the rectal route (PRV RR) on day 20 (D20). Two-tailed unpaired, nonparametric Mann-Whitney tests were conducted for A and B. For E and F, student's *t* tests were performed for statistical analysis (*, $P < 0.01$; **, $P < 0.001$; ***, $P < 0.0001$; ns, no significance).

TABLE 1 Metal-conjugated antibodies used for mass cytometry

No.	Metal conjugate (isotopic label)	Target epitope	Antibody clone	Source	Identifier
1	152Sm	CD3e	145-2C11	Fluidigm	3152004B
2	148Nd	CD11b (Mac-1)	M1/70	Fluidigm	3148003B
3	142Nd	CD11c	N418	Fluidigm	3142003B
4	89Y	CD45	30-F11	Fluidigm	3089005B
5	168Er	CD8a	53-6.7	Fluidigm	3168003B
6	145Nd	CD4	RM4-5	Fluidigm	3145002B
7	176Yb	CD45R (B220)	RA3-6B2	Fluidigm	3176002B
8	150Nd	Ly-6C	HK1.4	Fluidigm	3150010B
9	141Pr	Ly-6G	1A8	Fluidigm	3141008B
10	170Er	CD80 (B7-1)	16-10A1	BioLegend	104735
11	149Sm	CD19	6D5	Fluidigm	3149002B
12	147Sm	CD317	eBio927	Fisher (eBioscience)	50-145-15

characterized, attenuated ZIKV PRVABC59 mutant B strain lacking a glycosylation site (Asn 154 substituted with Thr) in the envelope region (Env-mB) (39, 40). Control mice received PBS (unprimed group). Subcutaneous infection with Env-mB resulted in a nonlethal, self-limiting infection with significantly reduced viremia compared to wild-type ZIKV infection (data not shown).

Following challenge, unprimed control mice lost significant body weight and had up to a 60% mortality rate by day 12 (Fig. 6A and B). In the PRV-primed mice, we did not observe weight loss or any neurological symptoms or signs of disease (limb weakness, partial or total hind-limb paralysis, and seizures). Moreover, this group had 100% complete protection. Although the Env-mB-primed mice maintained their body weights at significantly lower levels than PRV-primed mice, 80% of mice were protected from lethal challenge by day 12 (Fig. 6B). Both PRV- and Env-mB-primed groups showed reduced viremia at 3 days postsubcutaneous ZIKV challenge (Fig. 6C). PRV-primed mice were completely protected and had undetectable viremia at 7 days postsubcutaneous ZIKV challenge compared to the unprimed control group (Fig. 6C). However, 80% of animals in the attenuated, Env-mB-primed group were protected during challenge and had a significant 5-log reduction of serum viral titers relative to unprimed mice at 7 dpi (Fig. 6C). Furthermore, both mucosal-primed groups developed comparable ZIKV-specific neutralizing serum antibody responses (Fig. 6D). Immunohistochemistry analysis showed that unprimed mice had significantly higher levels of CD45-expressing cells in the brain (Fig. 6E and F). Thus, PRV-primed and Env-mB-primed mice were protected from ZIKV-mediated neuroinflammation. Two animals in the Env-mB-primed group showed low-grade $CD45^+$ inflammatory cell infiltrates in the brain (Fig. 6E and F), suggesting significant but partial protection from wild-type ZIKV virus challenge.

To further characterize the cellular and humoral immune responses mounted against ZIKV, we performed mass cytometry on cells isolated from spleens of mice following mucosal priming and after subcutaneous ZIKV challenge at 3 and 7 days (Fig. 7A). Multidimensional t-SNE plots indicate global dynamic changes of immune cell populations after ZIKV challenge (Fig. 7A). Unprimed control mice had significantly higher numbers of monocytes and neutrophils at 3 days postsubcutaneous ZIKV challenge (Fig. 7B). Mucosal-primed mice had significantly higher $CD4^+$ and $CD8^+$ T-cell responses at days 3 and 7 than unprimed mice (Fig. 7B). Env-mB-primed mice had significantly higher $CD4^+$ and $CD8^+$ T-cell responses than PRV-primed mice on day 3. However, a stronger B-cell response was observed for the PRV-primed group at this same time point. In addition, rectal immunization resulted in higher-memory $CD4^+$ and $CD8^+$ T-cell responses at 3 and 7 days postsubcutaneous ZIKV challenge (Fig. 7B). Interestingly, Env-mB-primed mice showed significantly higher dendritic cell responses relative to both unprimed and PRV-primed mice groups at 3 and 7 days postsubcutaneous ZIKV challenge. These results suggest that glycosylation of ZIKV envelope results in differential cellular immune responses that could be due to its inefficient infection of DC-SIGN lectin-expressing dendritic cells (40, 41). Overall, our results show that mucosal

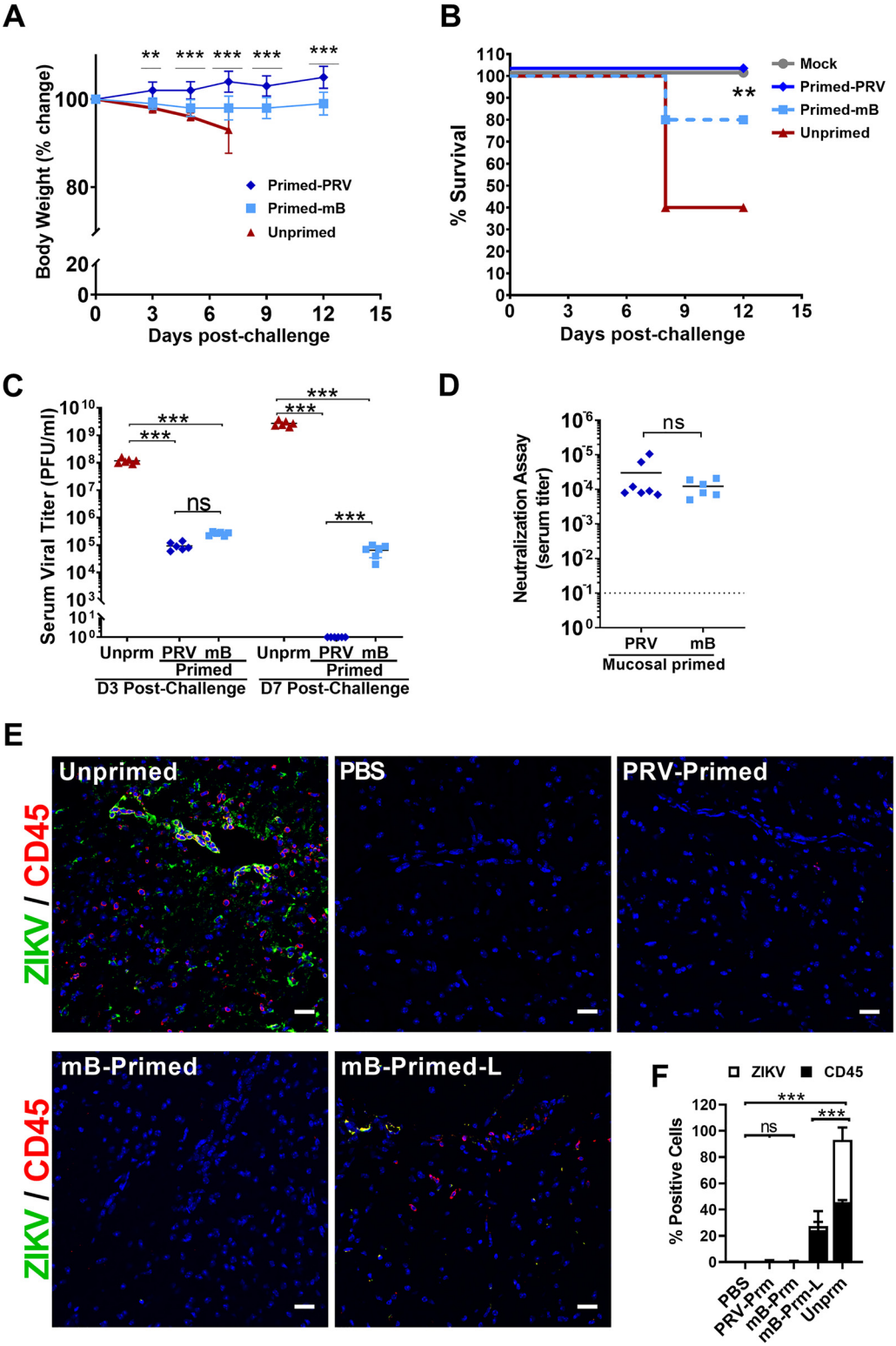

FIG 6 Mucosal priming with ZIKV via the rectal route leads to developing protective immunity. Percent body weight change (A) and percent survival (B) of unprimed (PBS) and mucosally ZIKV-primed mice (wild-type ZIKV PRVABC59 [Primed-PRV] or Env-mutant B virus [Primed-mB]) for 21 days via rectal route, followed by subcutaneous wild-type ZIKV challenge (dose 1×10^6 PFU/mouse; $n = 6$ mice per group). In the Kaplan-Meier survival graph, lines are nudged slightly for better visualization. (C) Serum viral titer of unprimed and primed mice at days 3 (D3) and 7 (D7) postsubcutaneous ZIKV challenge. (D) Serum neutralization titer of PRV- and mB-primed mice 7 days postsubcutaneous ZIKV challenge. (E) Immunohistochemistry analysis of brain sections for $CD45^+$ inflammatory cells (red) and ZIKV-Env antigen-positive cells (green). The brain tissues of unprimed mice exhibited heavy infiltration of inflammatory cells. A subset of two mice in the

(Continued on next page)

ZIKV infection elicits protective humoral and cellular immune responses that control systemic ZIKV replication and spread to restrict neuroinflammation.

DISCUSSION

This study provides a detailed immunopathological characterization of the rectal route of ZIKV transmission. The outcome of ZIKV infection can be determined by transmission bottlenecks for virus replication and dissemination from the portal of entry, thus leading to differences in systemic viral spread, which correlate with the neuroinvasive pathogenic outcome and increased cell death observed in the brains of subcutaneously infected mice at 7 dpi. The pathogenic differences observed between the two routes of infection can be attributed to the delay caused by the mucosal barrier to viral entry, immune priming at the intestinal-mucosal interface, and the altered splenic innate and/or adaptive immune responses against ZIKV infection. A caveat of our study is that the *Ifnar1*$^{-/-}$ mouse model has a deficient type I IFN innate immune system. Thus, this model may or may not reflect immunological responses observed in humans. Although this model lacks type 1 IFN response, it has competent B- and T-cell responses. Hence, this immunocompromised mouse model is useful in providing deeper insights into Zika virus pathogenesis and the resulting immunological responses to infection within different tissue microenvironments and in the development and testing of potential vaccine candidates. We have previously used this animal model system to elucidate the role of the Hippo signaling pathway in modulating ZIKV replication and neuroinflammation (42) and to describe the Zika-mediated metabolic changes occurring during infection (43). Moreover, the high dose of ZIKV used to inoculate mice via the subcutaneous route resulted in an accelerated systemic infection and an acute neuropathological outcome, whereas rectal ZIKV inoculation led to subclinical, nonneurological disease outcomes. Therefore, the dose of viral inoculum, duration of exposure, and the route of transmission can contribute to differential viral dissemination kinetics and disease outcome.

Our results are consistent with a different study which showed that intra-anal inoculation with ZIKV results in systemic infection of *Ifnar*1$^{-/-}$ mice (36). However, this study reported that the rectal route of ZIKV infection results in mortality and mice exhibit neurological signs of disease (36). Differences in clinical and pathological disease observed may be due to methodological approaches, such as exposure length to ZIKV via the rectal route (Li et al. reported 5 to 10 min, while we exposed mice for 4 min) and a distinction in the viral strain used. Our study of mucosal ZIKV transmission through the rectal route may model human ZIKV disease presentation, where 80% of infected individuals present subclinical and asymptomatic outcomes. In addition, Li et al. showed that ZIKV-specific IgG and IgM responses were detected at 7 days post-intra-anal ZIKV inoculation (36). Our study highlights the early cellular innate immune responses developed in the rectal mucosa following 1 and 3 days of rectal ZIKV inoculation. We provide evidence that dendritic cells are one of the primary targets of ZIKV infection in the rectal mucosa. We also determined that significantly higher levels of MCP-1^{+} cells are observed in the rectal mucosa following 3 days of rectal ZIKV inoculation, which can further mediate the recruitment of innate immune cells to the site of infection.

The rectal route of immunization against rotavirus virus-like particles (44) or hepatitis A virus vaccine (45) has been shown to elicit strong systemic humoral responses. Our model system of rectal immunization can be used as a platform to further understand humoral mucosal immunity and/or related antigen-specific T-cell memory

FIG 6 Legend (Continued)
mB-Primed group (mB-Primed-L) had low-grade inflammation in the brain compared to the unprimed group, and a representative image is shown. Images were collected at ×20 magnification; scale bar, 25 μm. (F) The percentage of CD45^{+} or ZIKV-Env-positive cells quantified in brain sections of mice. IHC images of brain sections from 3 to 5 mice were analyzed using the ImageJ Cell counter program. The percent positive cells was calculated from over 600 total cells counted per group. Two-way ANOVA with Sidak multiple-comparison tests were conducted for statistical analysis. ***, $P < 0.0001$; ns, no significance.

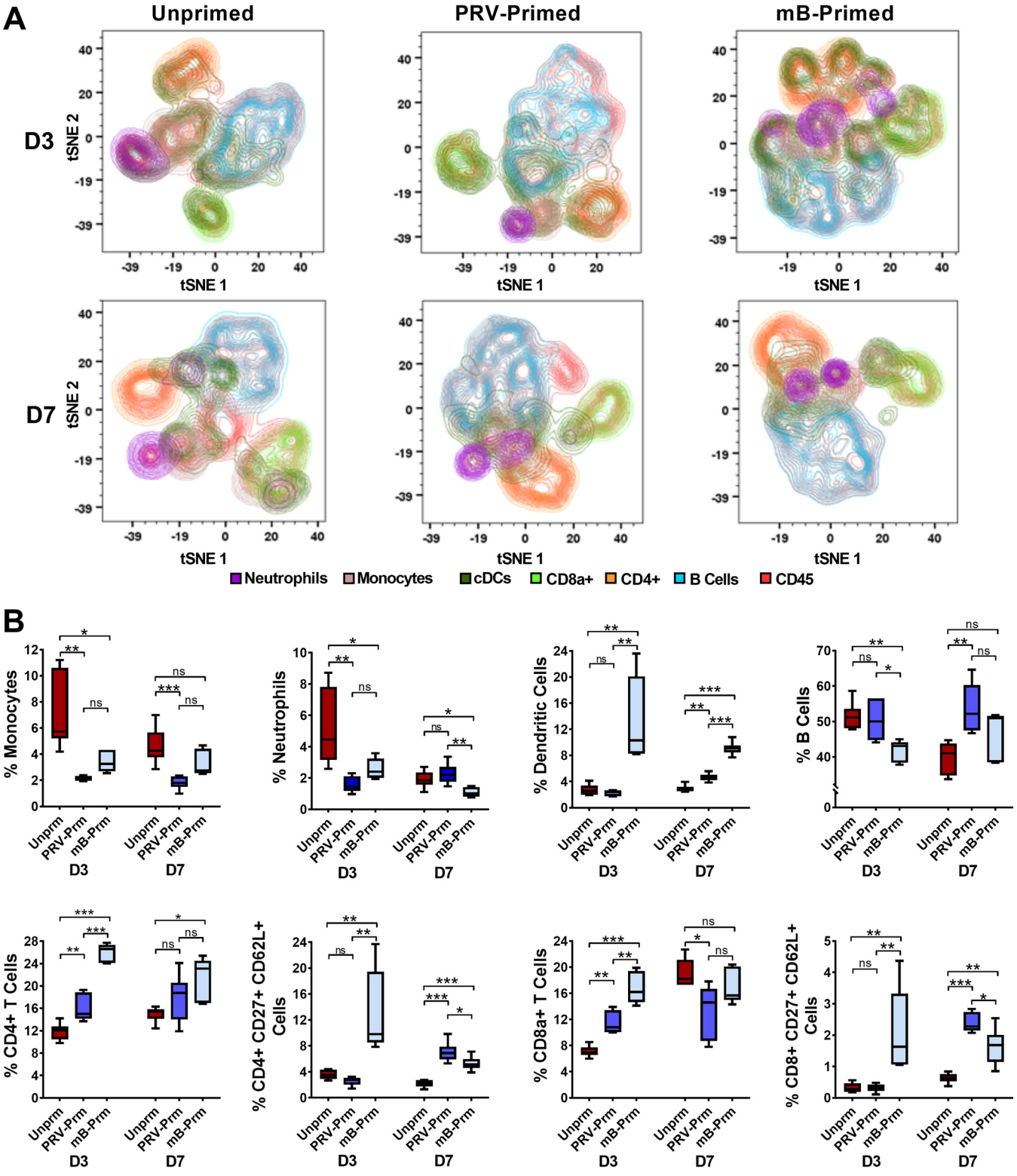

FIG 7 Rectal ZIKV immunization leads to protective immune responses against subcutaneous ZIKV challenge. (A) t-SNE plots showing spatially distinct immune cell populations in the spleens of unprimed and mucosally primed (PVR-Primed and mB-Primed, respectively) mice after 21 days of rectal immunization with ZIKV, followed by subcutaneous ZIKV challenge for 3 and 7 days. Results are representative of one of two independent experiments. (B) The percentage of splenic monocytes, neutrophils, dendritic cells, B cells, $CD4^+$ T cells, memory $CD4^+$ T cells ($CD4^+$ $CD27^+$ $CD62L^+$), $CD8a^+$ T cells, and memory $CD8^+$ T cells ($CD8^+$ $CD27^+$ $CD62L^+$) determined for unprimed and primed animals (PRV-Prm and mB-Prm, respectively) at D3 and D7 postsubcutaneous ZIKV challenge. One-way ANOVA with Tukey's multiple-comparison tests were conducted. *, $P < 0.01$; **, $P < 0.001$; ***, $P < 0.0001$; ns, no significance.

responses developed against ZIKV. The anorectal route could represent an epidemiologically relevant transmission reservoir for ZIKV in communities with high prevalence of unprotected anal sex practices. Further studies that examine the epidemiological and clinical consequences of the rectal route of ZIKV transmission will be critical for better understanding the pathophysiology of ZIKV in the mucosal microenvironment of humans. Mucosal immunization of ZIKV via prime and booster immunization approaches can be further developed to prevent future ZIKV outbreaks.

MATERIALS AND METHODS

Ethics statement. This study was performed in strict accordance with the recommendations of the guide for the care and use of laboratory animals (48). All animal experiments were conducted under approved Institutional Animal Care Use Committee (IACUC) protocols at the Cedars-Sinai Medical Center and the University of California, Los Angeles.

Cell lines and virus. The *Aedes albopictus* mosquito C6/36 cell line (CRL-1660 cell line from ATCC) was used for virus propagation. C6/36 cells were maintained at 28°C in Dulbecco's modified Eagle's medium (DMEM) (Sigma-Aldrich) supplemented with 10% heat-inactivated fetal bovine serum (FBS) (Gemini), 100 U/ml penicillin (Gibco), and 100 μg/ml streptomycin (Gibco). Vero cells were obtained from ATCC and were cultured in DMEM supplemented with 10% heat-inactivated FBS, 100 U/ml penicillin (Gibco), 100 μg/ml streptomycin, 1× GlutaMax (Gibco), and 20 mM HEPES (Gibco). The wild-type ZIKV PRVABC59 strain was received from the Centers for Disease Control (CDC). A previously characterized attenuated ZIKV PRVABC59 mutant strain lacking a glycosylation site (Asn 154 substituted with Thr) in the envelope region (Env-mB) was used (40). Working ZIKV stocks were prepared by infecting C6/36 cells. Supernatants were collected and centrifuged at 200 × *g* at 4°C for 10 min to remove cellular debris. The supernatant was then aliquoted and frozen at −80°C.

Quantification of ZIKV by plaque assay. Vero cells were plated (1×10^5 cells/well) on 12-well plates. Virus supernatants from C6/36 cells were used to titer virus from 10-fold serial dilutions in DMEM. Dilutions were added to Vero cell monolayers at 37°C for 4 h. After the incubation time, 400 μl of complete medium was added. Two days following the infection, plaques were counted, as previously described (46).

Rectal inoculation of *Ifnar1*$^{-/-}$ mice. Specific-pathogen-free *Ifnar1*$^{-/-}$ mice (B6.129S2-*Ifnar1*^{tm1Agt}/Mmjax) of congenic C57BL/6 genetic background were purchased from the Jackson Laboratory (derived by Mutant Mouse Resource and Research Centers [MMRRC] supported by NIH). Four- to six-week-old *Ifnar1*$^{-/-}$ mice were rectally inoculated with PBS or ZIKV (PRVABC59; isolated in Puerto Rico in 2015) while anesthetized with isoflurane ($n = 6$ mice per group). Briefly, a calginate swab was used to remove fecal stains from the anal orifice. Each mouse was inoculated with 1×10^6 PFU in a volume of 20 μl using a sterile smooth pipette tip (after passing or penetrating through the anal orifice). Mice were kept with the rectum facing upwards for 2 to 4 min to reduce leakage of the inoculum. Survival, weight loss, and clinical symptoms were monitored for 1, 3, 7, and 21 days postrectal inoculation (dpi). At the indicated times, mice were humanely euthanized by deep anesthesia with isoflurane followed by cervical dislocation. Blood was collected by direct cardiac puncture while the mouse was under isoflurane anesthesia. The mouse was then subjected to whole-body perfusion through the transcardial route with 1× PBS. To measure ZIKV viremia, 250 μl of blood was collected. Briefly, blood was centrifuged at 2,000 rpm for 15 min. Serum was stored at −80°C. Total RNA was extracted from serum using the viral RNA minikit (Qiagen). The rectum, testes, seminal vesicles, spleen, inguinal and mesenteric lymph nodes, and brain were harvested to measure viral load and cellular gene expression, as well as for immunohistochemistry. Tissues were removed from uninfected (PBS) or ZIKV-infected mice and dissected in thirds for fixation in 10% neutral buffered formalin for pathology, 4% paraformaldehyde for immunohistochemistry, or RNA*later* (Thermo Fisher Scientific) for RNA isolation.

Subcutaneous inoculation of *Ifnar1*$^{-/-}$ mice. For subcutaneous infections with ZIKV (SC ZIKV), 4- to 6-week-old *Ifnar1*$^{-/-}$ mice (A129) were inoculated with PBS ($n = 5$ to 6 mice) or ZIKV (1×10^6 PFU per mouse in a total volume of 40 μl) ($n = 5$ to 6 mice) in the hind-limb region. Blood was collected for viremia, and tissues were collected as described above.

Rectal mucosal ZIKV immunization and subcutaneous ZIKV challenge. At day 0, 12- to 14-week-old *Ifnar1*$^{-/-}$ mice (A129) of mixed sex were mucosally primed with wild-type ZIKV PRVABC59 (1×10^5 PFU/mouse) or with an attenuated ZIKV Env-mB strain (1×10^5 PFU/mouse) through the rectal route ($n = 6$ mice per group). PBS-inoculated mice were included as the unimmunized control group. At 3 weeks postrectal ZIKV immunization, control and both primed and unprimed groups were challenged with wild-type ZIKV PRVABC59 virus (1×10^6 PFU/mouse) through the subcutaneous route. Mice were weighed daily and closely monitored for health conditions and any neurological signs. For survival studies, animals were followed for 12 days. For assessing immune responses and viral load, blood and tissues were collected at 3 and 7 days postsubcutaneous ZIKV challenge. Cells isolated from the spleen were subjected to mass cytometry analysis. Serum was used for neutralization assays or viral titer assessment.

Histology. Brain tissues were placed in 10% neutral buffered formalin for 3 to 7 days and transferred to 70% ethanol. Tissue was then processed and embedded in paraffin, and sections were cut at 5 μm and stained with hematoxylin and eosin (H&E) at the Cedars-Sinai Research Histology and Molecular Pathology Core. Slides were evaluated in a blinded manner by a pathologist (S.F.) at UCLA. Evaluation

TABLE 2 RT-qPCR primer sequences

Primer	Forward	Reverse
ZIKV	AAGTACACATACCAAAACAAAGTGGT	TCCGCTCCCCCTTTGGTCTTG
Mouse *IL-6*	CAAAGCCAGAGTCCTTCAGAG	GTCCTTAGCCACTCCTTCTG
Mouse *OAS-1*	AGAGATGCTTCCAAGGTGC	ACTGATCCTCAAAGCTGGTG
Mouse *IL-10*	CCCTTTGCTATGGTGTCCTTTC	AGGATCTCCCTGGTTTCTCTTC
Mouse *MCP-1*	AGTAGGCTGGAGAGCTACAA	GTATGTCTGGACCCATTCCTTC

was conducted for uninfected (PBS) and infected brain tissue sections (rectal and subcutaneous routes of infection) at 7 dpi.

RNA sample preparation and RT-qPCR. To determine levels of virus in tissues of control and infected mice, tissues were placed in RNAlater (Thermo Fisher Scientific) immediately after harvest and stored at −80°C. Tissues were homogenized, and RNA was extracted using Trizol as per the manufacturer's instructions (Thermo Fisher Scientific). Total RNA was isolated from each sample. RNA was quantified using a NanoDrop 1000 spectrophotometer (Thermo Fisher Scientific). cDNA was prepared from 1 μg of RNA using random hexamer primers and the SuperScript III reverse transcriptase kit (Thermo Fischer Scientific). qPCR was performed using SYBR green ROX supermix (Life Technologies) and an Applied Biosystems QuantStudio 12K flex real-time PCR system (Thermo Fisher Scientific) or SSOAdvanced universal SYBR green supermix (Bio-Rad) using a CFX384 touch real-time PCR detection system (Bio-Rad). Briefly, amplification was performed using 10-μl volume reactions in a 384-well plate format with the following conditions: 95°C for 30 sec for polymerase activation and cDNA denaturation, then 40 cycles at 95°C for 15 s and 60°C for 1 min, with a melt-curve analysis at 65 to 95°C and 0.5°C increments at 2 to 5 s/step. The relative concentration of each transcript was calculated using the $2^{-\Delta CT}$ method, and glyceraldehyde 3-phosphate dehydrogenase (GAPDH) threshold cycle (C_T) values were used for normalization. The basal mRNA level in tissue from the PBS-inoculated group was normalized to 1, and the fold change relative to PBS was determined for each infected tissue type. The qPCR primer pairs for mRNA transcript targets are provided in Table 2. ZIKV RNA transcript levels were quantified by comparing them to a standard curve generated using serial 10-fold dilutions (10^0 to 10^{10} copies) of a ZIKV NS5 gene-containing plasmid. ZIKV RNA levels were expressed as ZIKV genome copies per 1 μg of RNA using the standard curve.

Immunohistochemistry. Tissue was fixed in 4% paraformaldehyde (PFA) for an hour, washed once, and transferred to PBS. Tissues were then submerged in 10% and 20% sucrose for an hour and 30% sucrose overnight at 4°C. Tissue was then embedded in OCT (Fisher Healthcare) and stored overnight at −80°C. Tissues were cut (7 to 10 μm thick) using a Leica cryostat microtome and mounted on Superfrost precleaned microscope slides (VWR) or poly-L-lysine-coated German glass round coverslips (14 mm, no. 1) (Electron Microscopy Services). Sections were washed once with 1× PBS to rehydrate tissue for 10 min. Three to six drops of Fc receptor blocker (peptide based) were added over each tissue sample for 30 to 60 min at room temperature. Immunostaining was conducted in the presence and absence of an Fc receptor blocker, and no differences in the staining of immune cells were observed. Tissues were rinsed once with wash buffer (0.3% Triton X-100 and 0.01% sodium azide in 1× PBS) for 5 min and then permeabilized using primary or secondary incubation buffer (1% bovine serum albumin [BSA], 0.3% Triton X-100, and 0.01% sodium azide in 1× PBS) for 1 h at room temperature. Sections were then rinsed with wash buffer and blocked with 5% normal goat serum (vol/vol) (Cell Signaling Technology), 5% normal donkey serum (vol/vol) (Jackson ImmunoResearch), or both, depending on the host source for the fluorescently labeled secondary antibody used. Sequential or simultaneous incubation with unlabeled primary antibodies was then performed. For ZIKV staining, sections were incubated overnight at 4°C with a rabbit anti-flavivirus group antigen recombinant monoclonal antibody (clone D1-4G2-4-15 [4G2] at 1:1,000), which recognizes the fusion loop of domain II of the envelope (Env) protein of dengue, West Nile, Japanese encephalitis, and Zika viruses, or the rabbit polyclonal anti-Zika NS4B antibody (1:250). Antibodies used to immunostain immune cells in rectal and brain tissues are listed in Table 3. Anti-CD11b was used to immunostain monocytes, anti-CD11c and anti-DC-SIGN for dendritic cells, anti-F4/80 for macrophages, anti-CD4 for $CD4^+$ T cells, and anti-CD45 for $CD45^+$ leukocytes. Isotype controls for rabbit, rat, or Armenian hamster were used to measure levels of nonspecific background signals caused by primary antibodies. A second negative control (without primary antibody) was also tested.

Sections were rinsed three times with wash buffer and incubated with fluorescently labeled secondary antibody for 1 h at room temperature. Sections were then rinsed three times with wash buffer for 5 min and stained with DAPI (4′,6-diamidino-2-phenylindole dihydrochloride) (Thermo Fisher Scientific) at a dilution of 1:5,000 in 1× PBS for 10 min. Round coverslips with tissue sections were mounted on precleaned glass slides using Prolong gold antifade mountant (Thermo Fisher Scientific) and sealed with nail polish. Images were acquired using LSM 700 or LSM 780 confocal microscopes and Zeiss software programs available at the UCLA Eli and Edythe Broad Center of Regenerative Medicine and Stem Cell Research Microscopy Core at the Paul I. Terasaki Life Sciences or Center for Health Sciences buildings.

Enumeration of immune cells in the rectal mucosa and the brain. Automated counts of immune cells in rectal tissue were done for tissue collected days 1, 3, and 7 postinfection. Confocal images were taken at ×20 magnification, and 8 to 15 nonoverlapping regions were acquired for image analysis. Each area included glands with lamina propria. Images with lymphoid aggregates were excluded from the analysis, as not all sections had lymphoid aggregates. For results presented in Fig. 2G and I and Fig. 3A,

TABLE 3 Reagents or resources used in this study

Reagent	Source	Identifier or catalog no.
Rat anti-mouse CD4 (clone GK1.5) monoclonal antibody	Bio-Rad	MCA4635GA
Rat monoclonal anti-mouse CD8, clone YTS169.4	Abcam	ab22378
Purified rat anti-CD11b, clone M1/70	BD Pharmingen	553308
Purified Armenian hamster anti-CD11c, clone N418	BioLegend	117302
Mouse DC-SIGN/CD209 antibody	R&D Systems	MAB83451
Purified rat anti-F4/80, clone BM8	eBioscience	14-4801-81
Leaf purified Armenian hamster anti-MCP-1 antibody	BioLegend	505905
Rat anti-mouse CD45	Bio-Rad	MCA1031GA
Rabbit flavivirus group primary antibody (D1-4G2-4-15)	Novus	NBP2-52666
Zika virus NS4B protein antibody, rabbit polyclonal	GeneTex	GTX133311
Rat anti-EpCAM monoclonal antibody, clone G8.8	Thermo Fisher Scientific	14-5791-81
Cleaved caspase-3 rabbit monoclonal antibody, clone D175	Cell Signaling	9661S
Purified rat anti-mouse CD31, clone MEC 13.3	BD Pharmingen	550274
Polyclonal rabbit anti-GFAP	Agilent Dako	Z033429-2
Rabbit IgG isotype control	Thermo Fisher Scientific	02-6102
Rat IgG isotype control	Invitrogen	31933
Mouse IgG isotype control	Invitrogen	10400C
Armenian hamster IgG isotype control	BioLegend	400902
Goat anti-rabbit Alexa Fluor 488	Thermo Fisher Scientific	A-11008
Goat anti-mouse Alexa Fluor 555	Thermo Fisher Scientific	A32727
Goat anti-rabbit Alexa Fluor 647	Thermo Fisher Scientific	A32733
Goat anti-rat Alexa Fluor 555	Thermo Fisher Scientific	A21434
Donkey anti-rabbit Alexa Fluor 555	Thermo Fisher Scientific	A31572
Donkey anti-rabbit Alexa Fluor 647	Jackson ImmunoResearch	711-605-152
Donkey anti-rat Cy3	Jackson ImmunoResearch	712-165-153
Goat anti-Armenian hamster Alexa Fluor 488	Abcam	ab173003
CD16/CD32, clone 93	eBioscience (Fisher)	50-124-40

cells were automatically counted from images of rectal tissue collected at ×20 magnification (dimensions, 408.2 μm by 408.2 μm) using the Cell Profiler program. Images were acquired from 2 different mice of 5 total mice from uninfected (PBS) and infected groups (RR versus SC ZIKV). For Fig. 6F, immunohistochemistry (IHC) images (×20 magnification) of brain sections from 3 to 5 mice were manually analyzed using the ImageJ cell counter program. Percent positive cells were calculated from over 600 total cells counted from four images for each mice group.

Neutralization Assay. Mice serum (15 μl/mouse) samples were heat inactivated at 55°C for 30 min. Serial 10-fold dilutions (10^1 to10^6) were prepared and incubated with 100 PFU of wild-type ZIKV PRVABC59 virus for 1 h at 37°C. Then, 100 μl of serum-virus complexes were added to Vero cell monolayers (48-well plate) (25,000 cells/well) and incubated for 2 h at 37°C/5% CO_2. The inoculum was removed, and the cells were washed twice (1× PBS) before adding fresh media (250 μl). The cells were then incubated for an additional 48 h. Viral plaques were then counted using a Leica phase-contrast inverted microscope.

Mass cytometry. Splenic cell populations were characterized by mass cytometry analysis. Metal-conjugated antibodies were used for high-dimensional description of immune markers at the single-cell level to characterize diverse immune cell populations (Table 1). We used the Maxpar cell surface staining protocol as per the manufacturer recommendations (Fluidigm) with minor modifications (47). Cells were isolated from the spleen to assess immunological responses under uninfected (mock) and ZIKV-infected conditions following rectal or subcutaneous inoculations. Briefly, the spleen was incubated in cold 1× PBS, cut into pieces, and mechanically disrupted using a syringe or 1-ml pipette tip. Homogenates were filtered through sterile 70-μm cell strainers (Falcon cell strainer; Fisher Scientific) with 10 ml of cold 1× PBS. Red blood cells were lysed using ACK lysing buffer (Gibco) for 2 min at room temperature. The cells were then resuspended in 8 ml of 1× PBS. Approximately 3×10^6 cells were aliquoted in a 1.5-ml screw-cap tube. Cells were centrifuged (300 × *g* for 5 min) and resuspended in 500 μl of 1× PBS with Cell-ID Cisplatin (Fluidigm) for 5 min. Cells were then resuspended in 50 μl of Maxpar staining buffer with Fc block solution (0.5 to 1 μg of CD16/CD32, clone 93; eBioscience) and were incubated for an additional 10 min. Subsequently, 50 μl of metal-conjugated antibody cocktail containing the antibodies of interest (with optimal concentrations), as listed in Table 1, was added and incubated for 30 min at room temperature. The cells were then subjected to two washes with Maxpar staining buffer before the addition of cell intercalation solution (Maxpar fix and perm buffer; Cell-ID Intercalator-Ir) and overnight incubation at 4°C. After the overnight incubation, cells were washed with Maxpar staining buffer, resuspended in water, and subjected to mass cytometry. Individual cells were ionized and analyzed by Helios CyTOF mass cytometer. Cell subpopulations were analyzed using the CyTOF software v6.7 (Fluidigm) and FlowJo software program (FlowJo, LLC).

Statistical analyses. All testing was done at the two-sided alpha level of 0.05. Data were analyzed for statistical significance using Student's *t* test or a parametric two-tailed unpaired Mann-Whitney *t* test to compare two groups (uninfected versus infected) with Graph Pad Prism software, version 8.3 (GraphPad Software, USA). Kaplan-Meier survival curves were analyzed by the Gehan-Breslow-Wilcoxon test. *P* values less than 0.05 were considered significant.

ACKNOWLEDGMENTS

We thank Neda Vishlaghi (Eli and Edythe Broad Center of Regenerative Medicine and Stem Cell Research at UCLA) for assistance with tissue cryosectioning, Sara Beshara for help with immunohistochemistry, and Sayan Paul and Alejandro J. Garcia for help with analyzing mass cytometry data. We also thank Samuel French for histopathological evaluation of brain tissue sections (Pathology and Laboratory Medicine and Surgical Pathology at UCLA), the Translational Pathology Core Laboratory (TPCL) at UCLA for H&E staining and digital image acquisition, and Ken Yamauchi, Ph.D. (Novitch lab) and the Eli and Edythe Broad Center of Regenerative Medicine and Stem Cell Research Microscopy Core at UCLA. We thank Aaron Brault and Brandy Russell of the Centers for Disease Control and Prevention (CDC), USA, for the PRVABC59 Zika virus strain.

Flow cytometry was performed in the UCLA Jonsson Comprehensive Cancer Center (JCCC) and Center for AIDS Research Flow Cytometry Core Facility, which are supported by the National Institutes of Health awards P30 CA016042 and 5P30 AI028697, and by the JCCC, the UCLA AIDS Institute, the David Geffen School of Medicine at UCLA, the UCLA Chancellor's Office, and the UCLA Vice Chancellor's Office of Research. This research was funded by Cedars-Sinai Medical Center's Institutional Research Award to V.A., the California Institute for Regenerative Medicine (CIRM) Quest–Discovery Stage Research Projects Grant (DISC2-10188) to V.A. at UCLA, and the UCLA Interdisciplinary Postdoctoral Training Grant (T32) in Virology and Gene Therapy to L.E.M. (5T32AI060567-14).

We declare no competing financial interests.

L.E.M. and V.A. designed the study. L.E.M., G.G., D.C., and V.A. performed experiments. L.E.M., G.G., D.C., and V.A. performed data analysis and interpretation. L.E.M., G.G., D.C., D.G., R.S., and V.A. wrote the manuscript.

REFERENCES

1. Ventura CV, Maia M, Bravo-Filho V, Góis AL, Belfort R, Jr. 2016. Zika virus in Brazil and macular atrophy in a child with microcephaly. Lancet 387:228. https://doi.org/10.1016/S0140-6736(16)00006-4.
2. Ventura CV, Maia M, Dias N, Ventura LO, Belfort R, Jr. 2016. Zika: neurological and ocular findings in infant without microcephaly. Lancet 387:2502. https://doi.org/10.1016/S0140-6736(16)30776-0.
3. Ventura CV, Maia M, Travassos SB, Martins TT, Patriota F, Nunes ME, Agra C, Torres VL, van der Linden V, Ramos RC, Rocha MA, Silva PS, Ventura LO, Belfort R, Jr. 2016. Risk factors associated with the ophthalmoscopic findings identified in infants with presumed Zika virus congenital infection. JAMA Ophthalmol 134:912–918. https://doi.org/10.1001/jamaophthalmol.2016.1784.
4. Ventura CV, Maia M, Ventura BV, Linden VV, Araujo EB, Ramos RC, Rocha MA, Carvalho MD, Belfort R, Jr, Ventura LO. 2016. Ophthalmological findings in infants with microcephaly and presumable intra-uterus Zika virus infection. Arq Bras Oftalmol 79:1–3. https://doi.org/10.5935/0004-2749.20160002.
5. Hills SL, Russell K, Hennessey M, Williams C, Oster AM, Fischer M, Mead P. 2016. Transmission of Zika virus through sexual contact with travelers to areas of ongoing transmission - continental United States, 2016. MMWR Morb Mortal Wkly Rep 65:215–216. https://doi.org/10.15585/mmwr.mm6508e2.
6. Moreira J, Peixoto TM, Siqueira AM, Lamas CC. 2017. Sexually acquired Zika virus: a systematic review. Clin Microbiol Infect 23:296–305. https://doi.org/10.1016/j.cmi.2016.12.027.
7. Russell K, Hills SL, Oster AM, Porse CC, Danyluk G, Cone M, Brooks R, Scotland S, Schiffman E, Fredette C, White JL, Ellingson K, Hubbard A, Cohn A, Fischer M, Mead P, Powers AM, Brooks JT. 2017. Male-to-female sexual transmission of Zika virus–United States, January–April 2016. Clin Infect Dis 64:211–213. https://doi.org/10.1093/cid/ciw692.
8. Deckard DT, Chung WM, Brooks JT, Smith JC, Woldai S, Hennessey M, Kwit N, Mead P. 2016. Male-to-male sexual transmission of Zika virus–Texas, January 2016. MMWR Morb Mortal Wkly Rep 65:372–374. https://doi.org/10.15585/mmwr.mm6514a3.
9. Davidson A, Slavinski S, Komoto K, Rakeman J, Weiss D. 2016. Suspected female-to-male sexual transmission of Zika virus - New York City, 2016. MMWR Morb Mortal Wkly Rep 65:716–717. https://doi.org/10.15585/mmwr.mm6528e2.
10. Atkinson B, Hearn P, Afrough B, Lumley S, Carter D, Aarons EJ, Simpson AJ, Brooks TJ, Hewson R. 2016. Detection of Zika virus in semen. Emerg Infect Dis 22:940. https://doi.org/10.3201/eid2205.160107.
11. Gaskell KM, Houlihan C, Nastouli E, Checkley AM. 2017. Persistent Zika virus detection in semen in a traveler returning to the United Kingdom from Brazil, 2016. Emerg Infect Dis 23:137–139. https://doi.org/10.3201/eid2301.161300.
12. Harrower J, Kiedrzynski T, Baker S, Upton A, Rahnama F, Sherwood J, Huang QS, Todd A, Pulford D. 2016. Sexual transmission of Zika virus and persistence in semen, New Zealand, 2016. Emerg Infect Dis 22:1855–1857. https://doi.org/10.3201/eid2210.160951.
13. Mansuy JM, Dutertre M, Mengelle C, Fourcade C, Marchou B, Delobel P, Izopet J, Martin-Blondel G. 2016. Zika virus: high infectious viral load in semen, a new sexually transmitted pathogen? Lancet Infect Dis 16:405. https://doi.org/10.1016/S1473-3099(16)00138-9.
14. Mansuy JM, Pasquier C, Daudin M, Chapuy-Regaud S, Moinard N, Chevreau C, Izopet J, Mengelle C, Bujan L. 2016. Zika virus in semen of a patient returning from a non-epidemic area. Lancet Infect Dis 16:894–895. https://doi.org/10.1016/S1473-3099(16)30153-0.
15. Atkinson B, Thorburn F, Petridou C, Bailey D, Hewson R, Simpson AJ, Brooks TJ, Aarons EJ. 2017. Presence and persistence of Zika virus RNA in semen, United Kingdom, 2016. Emerg Infect Dis 23:611–615. https://doi.org/10.3201/eid2304.161692.
16. Matheron S, d'Ortenzio E, Leparc-Goffart I, Hubert B, de Lamballerie X, Yazdanpanah Y. 2016. Long-lasting persistence of Zika virus in semen. Clin Infect Dis 63:1264. https://doi.org/10.1093/cid/ciw509.
17. Nicastri E, Castilletti C, Liuzzi G, Iannetta M, Capobianchi MR, Ippolito G. 2016. Persistent detection of Zika virus RNA in semen for six months after symptom onset in a traveller returning from Haiti to Italy, February 2016. Euro Surveill 21:30314. https://doi.org/10.2807/1560-7917.ES.2016.21.32.30314.
18. Oliveira Souto I, Alejo-Cancho I, Gascón Brustenga J, Peiró Mestres A, Muñoz Gutiérrez J, Martínez Yoldi MJ. 2018. Persistence of Zika virus in

semen 93 days after the onset of symptoms. Enferm Infecc Microbiol Clin 36:21–23. https://doi.org/10.1016/j.eimc.2016.10.009.
19. Aliota MT, Caine EA, Walker EC, Larkin KE, Camacho E, Osorio JE. 2016. Characterization of lethal Zika virus infection in AG129 mice. PLoS Negl Trop Dis 10:e0004682. https://doi.org/10.1371/journal.pntd.0004682.
20. Lazear HM, Govero J, Smith AM, Platt DJ, Fernandez E, Miner JJ, Diamond MS. 2016. A mouse model of Zika virus pathogenesis. Cell Host Microbe 19:720–730. https://doi.org/10.1016/j.chom.2016.03.010.
21. Miner JJ, Cao B, Govero J, Smith AM, Fernandez E, Cabrera OH, Garber C, Noll M, Klein RS, Noguchi KK, Mysorekar IU, Diamond MS. 2016. Zika virus infection during pregnancy in mice causes placental damage and fetal demise. Cell 165:1081–1091. https://doi.org/10.1016/j.cell.2016.05.008.
22. Rossi SL, Tesh RB, Azar SR, Muruato AE, Hanley KA, Auguste AJ, Langsjoen RM, Paessler S, Vasilakis N, Weaver SC. 2016. Characterization of a novel murine model to study Zika virus. Am J Trop Med Hyg 94:1362–1369. https://doi.org/10.4269/ajtmh.16-0111.
23. Khan S, Woodruff EM, Trapecar M, Fontaine KA, Ezaki A, Borbet TC, Ott M, Sanjabi S. 2016. Dampened antiviral immunity to intravaginal exposure to RNA viral pathogens allows enhanced viral replication. J Exp Med 213:2913–2929. https://doi.org/10.1084/jem.20161289.
24. Yockey LJ, Varela L, Rakib T, Khoury-Hanold W, Fink SL, Stutz B, Szigeti-Buck K, Van den Pol A, Lindenbach BD, Horvath TL, Iwasaki A. 2016. Vaginal exposure to Zika virus during pregnancy leads to fetal brain infection. Cell 166:1247–1256. https://doi.org/10.1016/j.cell.2016.08.004.
25. Govero J, Esakky P, Scheaffer SM, Fernandez E, Drury A, Platt DJ, Gorman MJ, Richner JM, Caine EA, Salazar V, Moley KH, Diamond MS. 2016. Zika virus infection damages the testes in mice. Nature 540:438–442. https://doi.org/10.1038/nature20556.
26. Uraki R, Hwang J, Jurado KA, Householder S, Yockey LJ, Hastings AK, Homer RJ, Iwasaki A, Fikrig E. 2017. Zika virus causes testicular atrophy. Sci Adv 3:e1602899. https://doi.org/10.1126/sciadv.1602899.
27. Ma W, Li S, Ma S, Jia L, Zhang F, Zhang Y, Zhang J, Wong G, Zhang S, Lu X, Liu M, Yan J, Li W, Qin C, Han D, Qin C, Wang N, Li X, Gao GF. 2017. Zika virus causes testis damage and leads to male infertility in mice. Cell 168:542. https://doi.org/10.1016/j.cell.2017.01.009.
28. McDonald EM, Duggal NK, Brault AC. 2017. Pathogenesis and sexual transmission of Spondweni and Zika viruses. PLoS Negl Trop Dis 11:e0005990. https://doi.org/10.1371/journal.pntd.0005990.
29. Kumar A, Jovel J, Lopez-Orozco J, Limonta D, Airo AM, Hou S, Stryapunina I, Fibke C, Moore RB, Hobman TC. 2018. Human Sertoli cells support high levels of Zika virus replication and persistence. Sci Rep 8:5477. https://doi.org/10.1038/s41598-018-23899-x.
30. Siemann DN, Strange DP, Maharaj PN, Shi PY, Verma S. 2017. Zika virus infects human Sertoli Cells and modulates the integrity of the in vitro blood-testis barrier model. J Virol 91:e00623-17. https://doi.org/10.1128/JVI.00623-17.
31. Kam YW, Leite JA, Lum FM, Tan JJL, Lee B, Judice CC, Teixeira DAT, Andreata-Santos R, Vinolo MA, Angerami R, Resende MR, Freitas ARR, Amaral E, Junior RP, Costa ML, Guida JP, Arns CW, Ferreira LCS, Renia L, Proenca-Modena JL, Ng LFP, Costa FTM, Zika-Unicamp Network. 2017. Specific biomarkers associated with neurological complications and congenital central nervous system abnormalities from Zika virus-infected patients in Brazil. J Infect Dis 216:172–181. https://doi.org/10.1093/infdis/jix261.
32. Foo SS, Chen W, Chan Y, Lee WS, Lee SA, Cheng G, Nielsen-Saines K, Brasil P, Jung JU. 2018. Biomarkers and immunoprofiles associated with fetal abnormalities of ZIKV-positive pregnancies. JCI Insight 3:e124152. https://doi.org/10.1172/jci.insight.124152.
33. Duggal NK, Ritter JM, Pestorius SE, Zaki SR, Davis BS, Chang GJ, Bowen RA, Brault AC. 2017. Frequent Zika virus sexual transmission and prolonged viral RNA shedding in an immunodeficient mouse model. Cell Rep 18:1751–1760. https://doi.org/10.1016/j.celrep.2017.01.056.
34. O'Connor MA, Tisoncik-Go J, Lewis TB, Miller CJ, Bratt D, Moats CR, Edlefsen PT, Smedley J, Klatt NR, Gale M, Fuller DH. 2018. Early cellular innate immune responses drive Zika viral persistence and tissue tropism in pigtail macaques. Nat Commun 9:3371. https://doi.org/10.1038/s41467-018-05826-w.
35. Botto-Menezes CHA, Neto AM, Calvet GA, Kara EO, Lacerda MVG, Castilho MDC, Stroher U, Antunes de Brito CA, Modjarrad K, Broutet N, Brasil P, Bispo de Filippis AM, Franca R, ZIKABRA Study Team. 2019. Zika virus in rectal swab samples. Emerg Infect Dis 25:951–954. https://doi.org/10.3201/eid2505.180904.
36. Li C, Deng YQ, Zu S, Quanquin N, Shang J, Tian M, Ji X, Zhang NN, Dong HL, Xu YP, Zhao LZ, Zhang FC, Li XF, Wu A, Cheng G, Qin CF. 2018. Zika virus shedding in the stool and infection through the anorectal mucosa in mice. Emerg Microbes Infect 7:169. https://doi.org/10.1038/s41426-018-0170-6.
37. Haddow AD, Nalca A, Rossi FD, Miller LJ, Wiley MR, Perez-Sautu U, Washington SC, Norris SL, Wollen-Roberts SE, Shamblin JD, Kimmel AE, Bloomfield HA, Valdez SM, Sprague TR, Principe LM, Bellanca SA, Cinkovich SS, Lugo-Roman L, Cazares LH, Pratt WD, Palacios GF, Bavari S, Pitt ML, Nasar F. 2017. High infection rates for adult macaques after intravaginal or intrarectal inoculation with Zika virus. Emerg Infect Dis 23:1274–1281. https://doi.org/10.3201/eid2308.170036.
38. Manangeeswaran M, Ireland DD, Verthelyi D. 2016. Zika (PRVABC59) infection is associated with T cell infiltration and neurodegeneration in CNS of immunocompetent neonatal C57Bl/6 Mice. PLoS Pathog 12:e1006004. https://doi.org/10.1371/journal.ppat.1006004.
39. Fontes-Garfias CR, Shan C, Luo H, Muruato AE, Medeiros DBA, Mays E, Xie X, Zou J, Roundy CM, Wakamiya M, Rossi SL, Wang T, Weaver SC, Shi PY. 2017. Functional analysis of glycosylation of Zika virus envelope protein. Cell Rep 21:1180–1190. https://doi.org/10.1016/j.celrep.2017.10.016.
40. Gong D, Zhang T-H, Zhao D, Du Y, Chapa TJ, Shi Y, Wang L, Contreras D, Zeng G, Shi P-Y, Wu T-T, Arumugaswami V, Sun R. 2018. High-throughput fitness profiling of Zika virus E protein reveals different roles for glycosylation during infection of mammalian and mosquito cells. iScience 1:97–111. https://doi.org/10.1016/j.isci.2018.02.005.
41. Carbaugh DL, Baric RS, Lazear HM. 2019. Envelope protein glycosylation mediates Zika virus pathogenesis. J Virol 93:e00113-19. https://doi.org/10.1128/JVI.00113-19.
42. Garcia Gjp S, Beshara S, Ramanujan VK, Ramaiah A, Nielsen-Saines K, Li MMH, French SW, Morizono K, Kumar A, Arumugaswami V. 2020. Hippo signaling pathway has a critical role in Zika virus replication and in the pathogenesis of neuroinflammation. Am J Pathol, in press. https://doi.org/10.1016/j.ajpath.2019.12.005.
43. Thaker SK, Chapa T, Garcia G, Jr, Gong D, Schmid EW, Arumugaswami V, Sun R, Christofk HR. 2019. Differential metabolic reprogramming by Zika virus promotes cell death in human versus mosquito cells. Cell Metab 29:1206–1216.e4. https://doi.org/10.1016/j.cmet.2019.01.024.
44. Parez N, Fourgeux C, Mohamed A, Dubuquoy C, Pillot M, Dehee A, Charpilienne A, Poncet D, Schwartz-Cornil I, Garbarg-Chenon A. 2006. Rectal immunization with rotavirus virus-like particles induces systemic and mucosal humoral immune responses and protects mice against rotavirus infection. J Virol 80:1752–1761. https://doi.org/10.1128/JVI.80.4.1752-1761.2006.
45. Mitchell LA, Galun E. 2003. Rectal immunization of mice with hepatitis A vaccine induces stronger systemic and local immune responses than parenteral immunization. Vaccine 21:1527–1538. https://doi.org/10.1016/s0264-410x(02)00699-0.
46. Contreras D, Arumugaswami V. 2016. Zika virus infectious cell culture system and the in vitro prophylactic effect of interferons. J Vis Exp 23:e54767. https://doi.org/10.3791/54767.
47. Chiang N, de la Rosa X, Libreros S, Serhan CN. 2017. Novel resolvin D2 receptor axis in infectious inflammation. J Immunol 198:842–851. https://doi.org/10.4049/jimmunol.1601650.
48. National Research Council (US) Committee for the Update of the Guide for the Care and Use of Laboratory Animals. 2011. Guide for the care and use of laboratory animals, 8th ed. National Academies Press (US), Washington, DC.